Study on the cleaning and cooling of solar photovoltaic panels using compressed airflow

Dacheng Li [*], Marcus King, Mark Dooner, Songshan Guo, Jihong Wang

School of Engineering, University of Warwick, Coventry CV4 7AL, UK

ARTICLE INFO

ABSTRACT

Solar photovoltaics (PV) are becoming one of the main sources of renewable energy to reduce carbon emissions of electricity supply. It is well recognised that dust accumulation and high temperatures result in a dramatic reduction in the performance of PV panels. To improve the efficiency of solar PV panels, a compressed air-based regulation method which can simultaneously clean and cool PV panels is studied and tested. A modelling study of the dust adhesion and detachment mechanism is conducted and the temperature variation caused by the air blowing process is analysed. Dynamic models of the compressed air release are derived which can be used to guide the design of the regulation system for increasing PV power output. A test system is developed for verifying various design and system parameters. The test results are used to validate the suitability of the modelling and illustrate how the inefficiency arising from soiling and high temperatures can be mitigated with the regulated compressed airflow. PV arrays serving in an arid region are adopted for this study and the increased energy yield arising from the cleaning and cooling effects is evaluated via the experimental test. The relationship between the airflow duration, various sizes of particles cleaning from the surface and power generation efficiency improvement is investigated to maximise the net power output increase from the PV panel. The results of this study can contribute to improving PV efficiency and help to realise decarbonisation in energy industry.

1. Introduction

Global solar power capacity increased from 25 GW at the beginning of 2010 to nearly 618 GW in 2019, and the overall investment in the solar energy sector within the Middle East and North Africa (MENA) region, which is ideal for photovoltaics (PV) installation, could reach $1 trillion between 2019 and 2023 (Middle east solar industry association, 2020). However, dust accumulation and high panel temperatures considerably reduce the performance of the solar panels, making them a less effective alternative energy source. For PV modules serving in the Eastern part of Saudi Arabia, the output power decreases by as much as 50% if uncleaned over a six-month period (Adinoyi and Said, 2013). In Kuwait, a 60% power reduction arising from panel soiling has been reported for the same duration (Sayigh et al., 1985). Additionally, PV modules convert only a small fraction of the solar irradiation into the electricity, the unconverted irradiation increases the temperature of the panel. When the temperature elevates, PV performance degrades because of the decrease in cell band gap (Said et al., 2018). For example, when heated from standard test temperature (around 20 °C) to 64 °C, an

efficiency reduction of 69% occurs in monocrystalline PV (Malik and Damit, 2003). Therefore, to improve the efficiency of the PV panels, it is critical to mitigate the combined effect of soiling and heating.

Various methods have been adopted to clean the surface of PV panels. Washing with water is a traditional method that removes dust and also cools the panel (Moharram et al., 2013). Despite the effectiveness, water cleaning is not suitable for arid desert regions for large-scale solar PV farms because of local water scarcity. Another basic practice for PV cleaning is manual or mechanically aided brushing (Al-Housani et al., 2019). However, rough brush cleaning can cause damage to the panel surface and lead to a reduction in efficiency and service life of the PV modules. Technologies such as surface vibration (Williams et al., 2007), acoustic waves (Alagoz and Apak, 2020), and electrody-namic dust shield (Mazumder et al., 2007; Kawamoto and Guo, 2018; Chesnutt et al., 2017) have been utilised to remove or prevent the dust falling on the solar cell and improve lifetime performance. However, relatively high costs and complex structures of these technologies limit their application in large scale, rural facilities. Additionally, a cooling effect is not available in these technologies and safety concerns in humid climates must also be considered. Therefore, a simple, anhydrous, and

---

Nomenclature

List of abbreviations

MENA	Middle East and North Africa
PV	photovoltaics
RMS	root-mean-square
RH	Relative Humidity
VdW	Vander Waals

List of nomenclature

A	Hamaker constant (J)
A_s	heat transfer area (m^2)
C_{Cu}	Cunningham correction factor
C_D	drag coefficient
C_f	skin friction coefficient
c_s	specific heat of the panel surface (kJ kg^{-1} K^{-1})
D_{pipe}	diameter of the pipeline (m)
E_{abs}	absorption efficiency (m^2 g^{-1})
E_{scat}	scattering efficiency (m^2 g^{-1})
f	near wall effect correction factor
f_m	wall effect correction factor
F_{ad}	adhesion force (N)
F_C	capillary force (N)
F_D	drag force (N)
F_E	electrostatic force (N)
F_G	gravitational force (N)
F_L	lift force (N)
F_{VdW}	Vander Waals force (N)
h	average convective heat transfer coefficient (kW m^{-2} K^{-1})
H	height of the solar PV panel (m)
H_0	closest distance between the surfaces (m)
i	ith thermocouple
k	thermal conductivity (W m^{-1} K^{-1})
K	$=1$, for the conductive plane
L	length of the solar PV panel (m)
L_{pipe}	length of the pipeline (m)
m_{cleand}	dust mass on the cleaned panel (kg)
m_{dust}	mass of the dust (kg)
m_s	mass of the panel surface (kg)
$\dot{m}_{air}$	mass flow rate of the air (kg s^{-1})
M_R	rolling moment (N m)
N_{PV}	number of solar PV panels
Nu	Nusselt number
P_a	ambient pressure (Pa)
P_{clean}	power output from the clean panel (kW)
P_{cleand}	power output from the cleaned panel (kW)
P_{soiled}	power output from the soiled panel (kW)
P_{loss}	pressure loss in the pipeline (Pa)
P_{noz}	working pressure of the nozzle (Pa)
Pr	Prandtl number
q	particle charge (C)
Q_{air}	flow rate of the air (m^3 s^{-1})
R	particle radius (m)
R_A	individual gas constant (kJ kg^{-1} K^{-1})
R_g	universal gas constant (kJ kmol^{-1} K^{-1})
R_r	contact radius (m)
Re	Reynolds number
Re_p	Reynolds number of the particle
T_a	ambient temperature (K)
T_{air}	temperature of the airflow (K)
T_{Back}	back temperature of the solar PV panel (K)
T_s	temperature of the panel surface (K)

T_{tank}	temperature of the air tank (K)
T_{Top}	top temperature of the solar PV panel (K)
U	uncertainty in the measurement (%)
V_{air}	air velocity (m s^{-1})
V_m	mean air velocity at the particle centre (m s^{-1})
V_s	shear velocity (m s^{-1})
V_{tank}	volume of the air tank (m^3)
W	width of the solar PV panel (m)
W_{cons}	power consumption (kWh)
W_{gain}	energy gain from cleaning and cooling effects (kWh)

Greek symbols

β	particle upscatter fraction
γ	isentropic coefficient
Γ	coefficient of wall condition
ΔP_{clean}	power improvement by the cleaning effect (kW)
$\Delta P_{cooling}$	power improvement by the cooling effect (kW)
ΔS	change of solar transmittance (% m^{-2})
Δt	air blowing time (s)
ε_0	vacuum permittivity (C^2 N^{-1} m^{-2})
η	power decrease coefficient per temperature unit (% K^{-1})
$\eta_{cleaning}$	cleaning rate (%)
η_{comp}	efficiency of the compressor (%)
η_{motor}	efficiency of the motor (%)
θ	solar PV panel inclined degree (°)
θ_1	top contact angle (°)
θ_2	bottom contact angle (°)
λ	molecular mean free path (m)
μ	friction coefficient
ξ	H_0/R
ρ	dust density (kg m^{-3})
ρ_{air}	air density (kg m^{-3})
τ	shear stress (Pa)
ν	kinetic viscosity (m^2 s^{-1})
ψ	liquid's surface tension (N m^{-1})

Subscripts

a	ambient
abs	absorption
ad	adhesion
air	air
back	back
C	capillary
clean	clean
cleaned	cleaned
comp	compressor
cons	consumption
Cu	Cunningham
D	drag
dust	dust
E	electrostatic
G	gravitational
gain	gain
L	lift
motor	motor
p	particle
pipe	pipe
s	surface
scat	scattering
tank	tank
Top	Top

low-cost solution should be investigated to effectively mitigate the soiling and heating impacts on the PV panels.

Using the turbulent airflow generated from the compressed air which neither consumes water nor makes physical contact with surface is an attractive PV cleaning method (Du et al., 2019). In addition to removing accumulated dust on the cell surface, the air can also help dissipate heat to keep the panel cool and thus increase the PV power output. This technology has a simple structure and relatively low cost, therefore, is suitable for a bulk solar PV farm in the MENA region. To achieve this, the theoretical guidance and an experimental basis for the design and control of the compressed air-based regulation system should be provided. However, few prior investigations have been conducted considering the simultaneous effect of cleaning and cooling using compressed airflow, and the gap between theoretical attempts and demonstration studies remains. Additionally, the aspects that influence the energy profit of this technology also need to be addressed to operate the system efficiently.

In this paper, mathematical modelling of the dust adhesion to the PV panel surfaces and the detachment under the turbulent airflow is studied. The temperature drop accompanying the cleaning process is analysed and the dynamic model of the compressed air discharging process is established. A test system of the regulation mechanism is developed to validate the proposed modelling and show the effectiveness of cleaning and cooling on the increase of PV power. Design of a regulation system for the PV arrays serving in arid regions is conducted and the improvement of the panel's performance is evaluated. In addition, the influence of the blowing duration and size of particles cleaned from the surface on the energy profit is investigated. After Conclusion, future work is suggested for further improvement of solar PV performance using compressed air-based regulation system.

2. Theoretical analysis and mathematical modelling

As depicted in Fig. 1, the compressed air-based regulation system has a simple structure, mainly composed of a compressed-air unit (a compressor, an air tank, and an air flow regulation valve) and nozzles. In a real application, a compressed-air unit can be designed for a group of PV arrays. The compressor is directly powered by the PV panels and the release of the compressed air from the tank is regulated by the valve to meet the mass flow requirements of cleaning and cooling. The spreading air from the nozzles installed at the edge of panels overlaps and forms a flake shape airflow, then carries away the dust and heat from the panel surface. Components used in the system are low-cost and highly-reliable standardised products. The system can be constructed using a fixed pipe assembly to transmit air to the panel and may be made as a mobile set of equipment to move to the location where cleaning and cooling is needed. This depends on applications and cost of the whole system.

2.1. Modelling of cleaning process

To facilitate the modelling work, the following assumptions are made first:

(1). The dust particles are spherical, and the adhesion occurs between the dust and panel surface which are both made of SiO_2.
(2). To fully utilise the gravitational force contributing to the dust removal from the tilting solar panel, the air blows over the panel surface in a tangential direction from top to bottom.
(3). The adhesion between dust particles and the gravity effect on airflow are neglected.

2.1.1. Adhesion model

Referring to Fig. 2, the main adhesion forces subject by the dust particles deposited on the PV panel surface include Vander Waals (VdW) forces (F_{VdW}), Electrostatic forces (F_E), and Capillary forces (F_C). To receive more solar radiation, the PV panel inclined degree θ according to
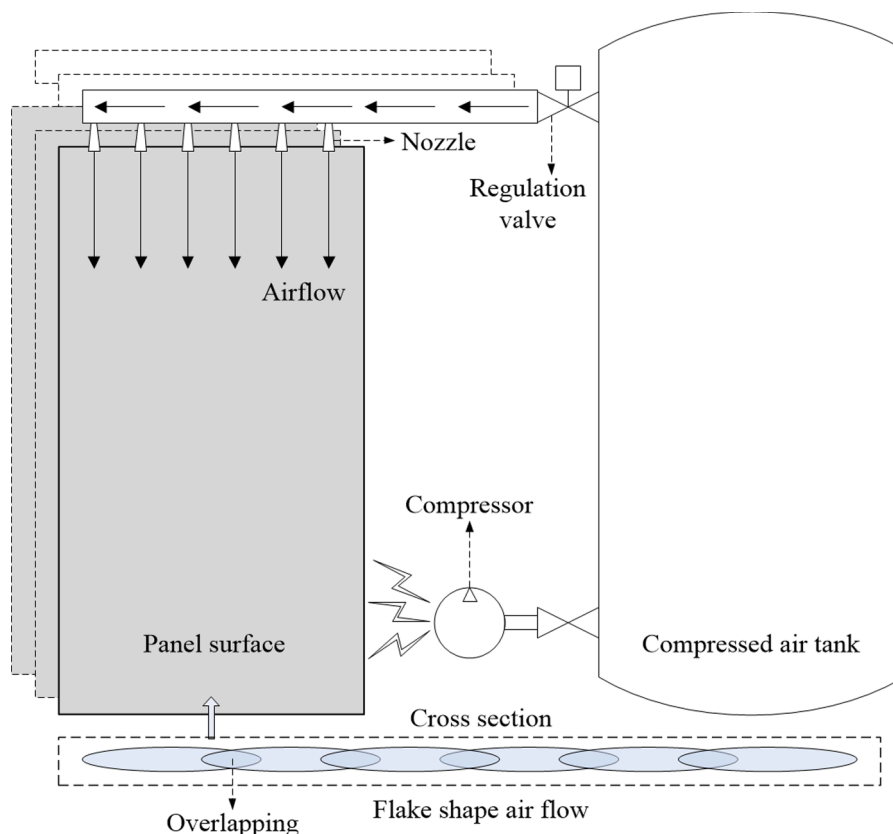

Fig. 1. Schematic diagram of compressed air-based regulation system for solar PV panel arrays.
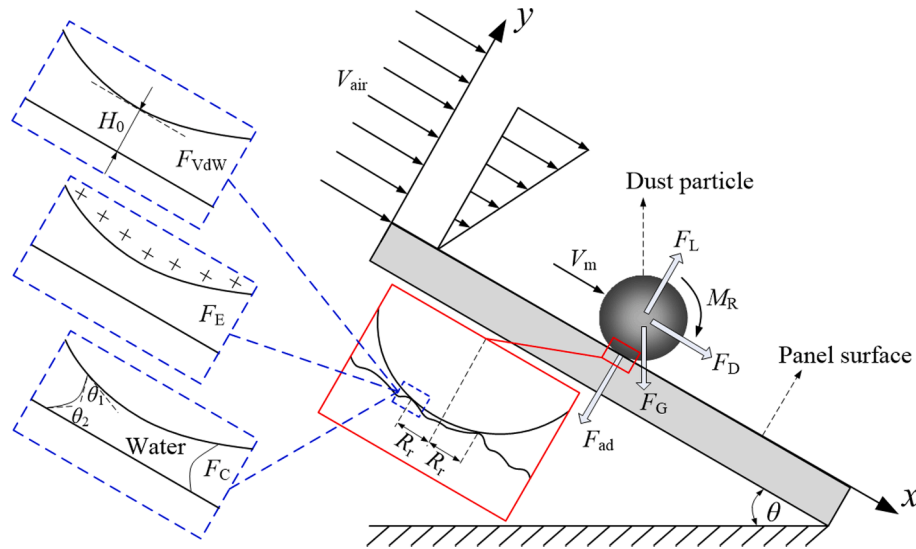
Fig. 2. Schematic diagram of force analysis for the particle on the inclined solar PV panel.

the located latitude (Shariah et al., 2002).

(a) Van der Waals forces

Arising from the interacting dipoles between two contacted bodies, VdW forces occur at the contact boundary of the dust particle and panel surface. In the low Relative Humidity (RH < 30%) and neutral electrostatic environment, this force can be regarded as the dominant force in adhesion (Li et al., 2006; Moutinho et al., 2017). When the surfaces of the particle and panel are smooth, VdW force can be written as (Hamaker, 1937)

$$F_{VdW} = A \frac{R}{6H_0^2} \qquad (1)$$

where A is Hamaker constant ($=7 \times 10^{-20}$ J for interaction between SiO_2 and SiO_2), R is the particle radius, and H_0 is the closest distance between the surfaces ($=0.3$ nm for minimum intermolecular distance). In the real situation, the surface of dust particle and solar panel have some roughness. The existence of nanoscale roughness results in adhesion reduction because of a decrease in the actual contact area and an increase in the distance between the bulk surfaces. When a spherical particle interacting with a much smaller scale of asperity, the VdW force becomes (Rumpf, 1990):

$$F_{VdW} = A \frac{R}{6H_0^2} \left[\frac{1}{1 + R/(1.48 \text{RMS})} + \frac{1}{(1 + 1.48 \text{RMS}/H_0)^2} \right] \qquad (2)$$

where RMS is the root-mean-square of the roughness.

(b) Electrostatic forces

The electrostatic forces acting on a charged dust particle can be either attractive or repulsive, depending on the conductivity of the panel surface and the permittivity of medium between the bulk surfaces (Brambilla et al., 2017). The force can be presented as (Crowley, 2008):

$$F_E = \frac{q^2}{16\pi\varepsilon_0 R^2} \left[\frac{1}{(\xi + \xi^2)(1 + 0.5 log(1 + 1/\xi))} \right] K \qquad (3)$$

where q is the particle charge, ε_0 is the vacuum permittivity ($=8.854 \times 10^{-12}$ C^2 N^{-1} m^{-2}), $\xi = H_0/R$, and $K = 1$ for the conductive plane.

(c) Capillary forces

Capillary forces arise between the hydrophilic surface of the panel and the particle owing to water condensation. As shown in Fig. 2, the concave meniscus of water pulls the particle towards the panel. According to (Ilse et al, 2018; Figgis et al, 2018), the force can present even at lower RH (30–40%) and is represented by

$$F_C = 2\pi R\psi(cos\theta_1 + cos\theta_2) \qquad (4)$$

where ψ is the liquid's surface tension ($=0.07275$ N m^{-1}), and θ_1 and θ_2 are the contact angle.

In arid and semi-arid climates, the diameter of dust settling on the PV panel surface is in the range of 2–64 μm (Ilse et al., 2018). To have an intuitive view of the particle adhesion, the variation of the forces with different particle size was studied according to Eqs. (1)-(4). As depicted in Fig. 3, the adhesion forces rise with the increased diameters and the magnitude under a certain dimension falls in the following relationship:

$$F_C > F_{AdW} > F_E$$

In a real situation, not all the above forces play important roles in the adhesion at the same time. When the humidity of surroundings increases, the VdW forces and electrostatic forces will considerably decrease because of the reduction of the Hamaker constant and the charge compensation (Ilse et al., 2018). On the other hand, calculated by Eqs. (1)-(2), the roughness of the panel surface induces a reduction of the VdW force. Taking the particle diameter 20 μm as an example, the VdW force decreased to 1.5% of that in the smooth condition at 100 nm RMS roughness. It is worth noting that for a very small or very large surface roughness, the situation is similar to a particle adhering to a smooth surface and the VdW force is close to the value calculated by Eq. (1).

Because of the repeated humid/dry cycles, needle-like fibrous structures form between particles and panel surface and result in cementation of dust (Ilse et al, 2016). In this case, mechanical brushing with water will come to the most feasible cleaning way (Gupta et al, 2019). Therefore, to prevent cementation, it is necessary to implement the cleaning before the ambient temperature becomes lower than the dew point at night (Kawamoto, 2020).

2.1.2. Detachment model

As shown in Fig. 2, when the air flows over the panel surface in a tangential direction, the drag force (F_D), rolling moment (M_R), and lift force (F_L) will exert on the dust particle. Referring to (Ahmadi and Guo, 2007), the air drag force can be expressed as
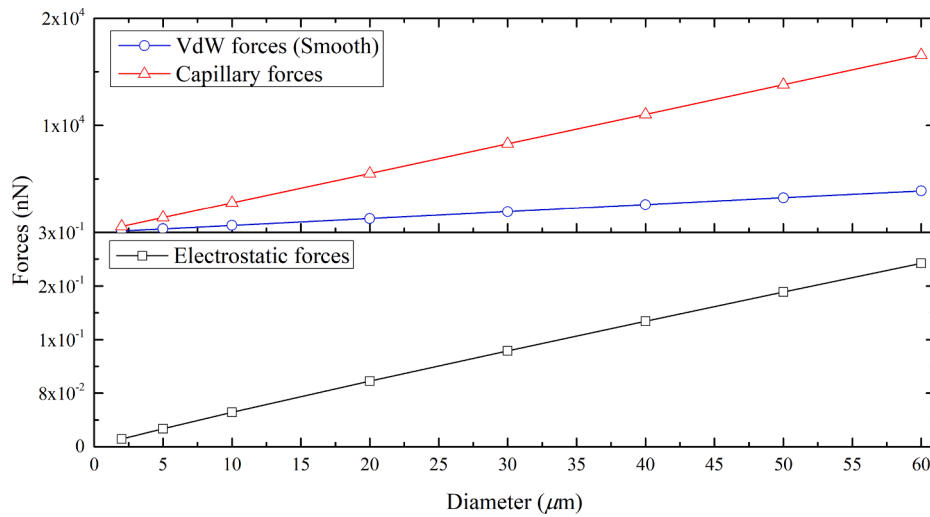
Fig. 3. Variation of adhesion forces with different particle diameter (particle charge $q = R \times 2 \times 10^{-12}$C (Hinds, 2012), $\theta_1 = 60°$, $\theta_2 = 45°$).

$$F_D = \frac{C_D f \rho_{air} \pi R^2 V_m^2}{2 C_{Cu}} \tag{5}$$

where C_D is the drag coefficient, $f = 1.7009$ is the correction factor for the near wall effect (Goldman et al., 1967), ρ_{air} is the air density, V_m is the mean air velocity at the particle centre, and C_{Cu} is the Cunningham correction factor. Among them:

$$C_D = \begin{cases} \frac{24}{Re_p}(1 + \frac{1}{6}Re_p^{2/3}) \ Re_p \leqslant 1000 \\ 0.44 \ 1000 < Re_p \leqslant 2 \times 10^5 \end{cases} \tag{6}$$

$$V_m = \frac{\Gamma R V_s^2}{\nu} \tag{7}$$

$$C_{Cu} = 1 + \frac{\lambda}{R}[1.257 + 0.4exp(-1.1R/\lambda)] \tag{8}$$

In Eqs. (6)–(8), V_s is the shear velocity, ν is the kinetic viscosity of air, λ is the molecular mean free path in the gas ($=6.9 \times 10^{-8}$ m), Γ is the coefficient of wall condition, and Re_p is the Reynolds number of the particle which can be presented as (Burdick et al., 2005)

$$Re_p = 2\Gamma \left(\frac{RV_s}{\nu}\right)^2 \tag{9}$$

Additionally, the rolling moment acting on the dust is given by (Ahmadi and Guo, 2007):

$$M_R = \frac{8\Gamma f_m \rho_{air} \pi R^3 V_s^2}{C_{Cu}} \tag{10}$$

where $f_m = 0.94399$ is the wall effect correction factor (Goldman et al., 1967). In addition, the lift force acting on the dust particle by the airflow can be obtained using the following equation (Ahmadi et al, 2007):

$$F_L = \frac{11.904 \rho_{air} R^4 V_s^4}{\nu^2} \tag{11}$$

Apart from the adhesion forces, dust particles also suffer from the gravitational force which is

$$F_G = \frac{4\pi R^3}{3}\rho g \tag{12}$$

where ρ is the dust density. Under the removing function of the forces and moments, three detachment modes for the dust particle are available:

Liftoff: $F_L \geqslant F_{ad} + F_G cos(\theta)$

Sliding: $F_D \geqslant \mu(F_{ad} + F_G cos(\theta) - F_L) - F_G sin(\theta)$

Rolling: $(F_D + F_G sin(\theta))\sqrt{(R^2 - R_r^2)} + M_R \geqslant (F_{ad} + F_G cos(\theta) - F_L)R_r$

$$\tag{13}$$

where F_{ad} is the adhesion force, R_r is the contact radius, and μ is the friction coefficient for the particle–surface interface.

To reach the shear velocity to remove the dust particle on the panel surface, the required air velocity needs to be determined. According to the air dynamics, the shear velocity and shear stress can be shown as:

$$V_s = \sqrt{\frac{\tau}{\rho_{air}}} \tag{14}$$

$$\tau = \frac{C_f \rho_{air} V_{air}^2}{2} \tag{15}$$

In the above equation, the skin friction coefficient is (Jiang et al., 2018)

$$C_f = 0.0592 Re_x^{-0.2} \tag{16}$$

where the Reynolds number $Re_x = V_{air}x/\nu$. Combining Eqs. (14)-(16), the air velocity can be shown as

$$V_{air} = \sqrt[1.8]{\frac{2V_s^2}{0.0592} \cdot \left(\frac{x}{\nu}\right)^{0.2}} \tag{17}$$

In the arid environment, VdW force and electrostatic force are determined as the main adhesion forces. To evaluate the ideal cleaning mechanism with less air consumption, the required shear and air velocity for each detachment mode for the dust on the smooth surface were obtained and compared (e.g. $\Gamma = 1.84$; $\mu=0.2$; $x = L = 1.211$ m, which was the length of the panel surface along the direction of the airflow). As shown in Figs. 4 and 5, the rolling mode was the favoured detachment mechanism for the dust which needed a lower airflow rate. On the other hand, the required velocity decreased with the increase of the particle size in each detachment mode. This reflects the fact that large size particles are easy to be removed than the smaller ones.

The influence of the dust deposition on the PV performance can be estimated using the reduction rate of the transmittance of visible solar energy to the PV module under per unit of dust mass (Bergin et al., 2017):

$$\frac{\Delta S}{m_{dust}} = -(E_{abs} + \beta E_{scat}) \tag{18}$$
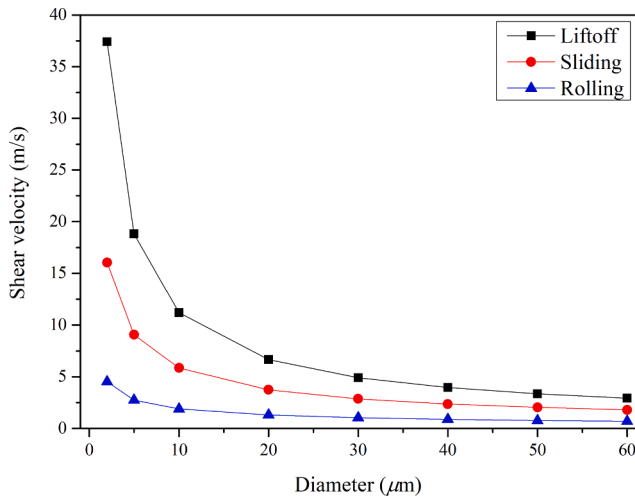
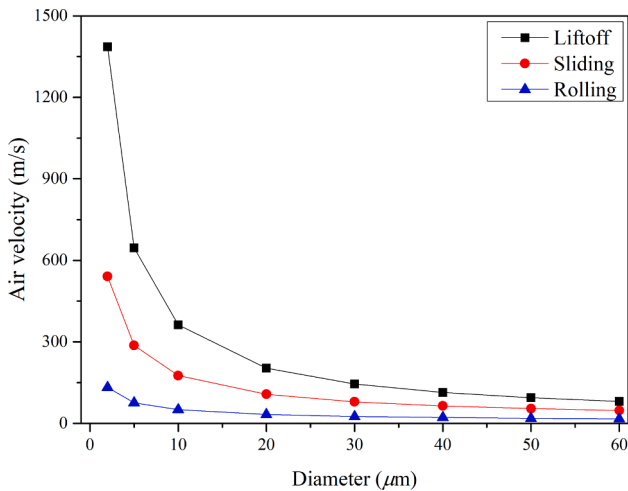**Fig. 4.** Shear velocity for particle detachment.

Fig. 5. Air velocity for particle detachment.

where ΔS is the change of solar transmittance, m_{dust} is the mass of the dust on the panel surface, E_{abs} and E_{scat} are the matter mass absorption and scattering efficiencies, respectively, and β is the particle upscatter fraction. Then, power improvement by the cleaning effect can be calculated as:

$$\Delta P_{clean} = (m_{dust} - m_{cleaned})(E_{abs} + \beta E_{scat}) \times P_{clean} \tag{19}$$

where m_{cleand} and P_{clean} are the dust mass on the cleaned panel surface and power output from the clean solar panel, respectively. Cleaning rate by the air blowing can be evaluated as:

$$\eta_{cleaning} = \frac{P_{cleaned} - P_{soiled}}{P_{clean} - P_{soiled}} \times 100\% \tag{20}$$

where P_{cleand} and P_{soiled} are the power output from the cleaned and soiled solar panel, respectively.

2.2. Modelling of cooling process

When the airflow blows off the dust, it also takes away the heat from the panel. The cooling process can be expressed by the following equation:

$$m_s c_s \frac{dT_s}{dt} = - hA_s(T_s - T_{air}) \tag{21}$$

where m_s and c_s are the mass and specific heat of the panel surface; h is the average convective heat transfer coefficient; A_s and T_s are the heat transfer area and temperature of the panel surface, respectively; and T_{air} is the airflow temperature. The convective heat transfer coefficient is presented as follows (Incropera et al., 2006):

$$h = \frac{Nu \cdot k}{L} \tag{22}$$

$$Nu = 0.0296 Re^{4/5} Pr^{1/3} \tag{23}$$

where k is the thermal conductivity and the Nu, Re, and Pr are the Nusselt number, Reynolds number, and Prandtl number, respectively. Under the initial condition $t = 0$ and $T_s = T_s^0$, Eq. (21) can be obtained as follows at any moment during the cooling process:

$$T_s = T_{air} + \left[exp(\frac{hA_s}{m_s c_s} t) \right]^{-1} (T_s^0 - T_{air}) \tag{24}$$

The PV power output improves with the decrease of the temperature and the magnitude can be quantified as

$$\Delta P_{cooling} = P(T_a)\left(1 - \int_{T_a}^{T} \eta dT \right) - P(T_s^0) \tag{25}$$

where T_a is the ambient temperature and η is the power decrease coefficient per temperature unit (Assi et al., 2012).

2.3. Modelling of compressed air release

Assuming no heat transfer occurs between the air tank and atmosphere, then the dynamic change of the pressure in the tank during discharging is:

$$\frac{dP_{tank}}{dt} = - \frac{\gamma T_{tank} R_g}{V_{tank}} N_{PV} \dot{m}_{air} \tag{26}$$

where γ is isentropic coefficient, T_{tank} and V_{tank} are the temperature and volume of the air tank, respectively, R_g is the universal gas constant, N_{PV} is the number of PV modules in the arrays, and $\dot{m}_{air}$ is the mass flow rate of the air. Considering the pressure loss in the pipeline, the initial air pressure in the tank is

$$P_{tank}^0 = \frac{\gamma T_{tank} R_g}{V_{tank}} N_{PV} \dot{m}_{air} \Delta t + P_{noz} + P_{loss} \tag{27}$$

where Δt is the air blowing time and P_{noz} is the working pressure of the nozzle. The pressure loss in the pipeline is represented as (Carello et al., 1998)

$$P_{loss} = 1.6 \times 10^3 Q_{air}^{1.85} \frac{N_{PV} L_{pipe}}{D_{pipe}^5 \cdot (P_{noz} + P_{loss})} \tag{28}$$

where Q_{air} is the flow rate of the air, L_{pipe} and D_{pipe} are the length and diameter of the transmission pipeline, respectively. Assuming an isentropic compression process, power consumption to obtain the compressed air is (Hartmann et al., 2012):

$$W_{cons} = m_{air} \frac{\gamma}{\gamma - 1} R_A T_a \left[\left(\frac{P_{tank}^0}{P_a} \right)^{\frac{\gamma-1}{\gamma}} - 1 \right] \frac{1}{\eta_{comp}} \cdot \frac{1}{\eta_{motor}} \tag{29}$$

where m_{air} is the mass of air, R_A is individual gas constant for air, P_a is the ambient pressure, and η_{comp} and η_{motor} are efficiencies of the compressor and motor, respectively.
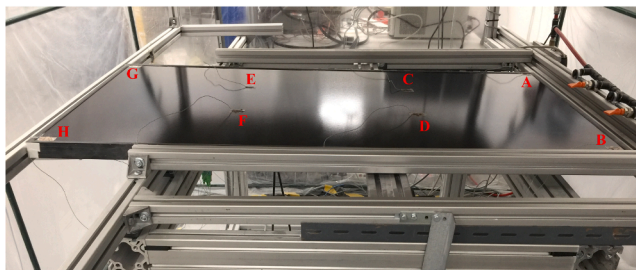
3. Experimental setting up

To validate the effectiveness of the proposed modelling and mitigation of soiling and heating by the compressed airflow, as shown in Fig. 6
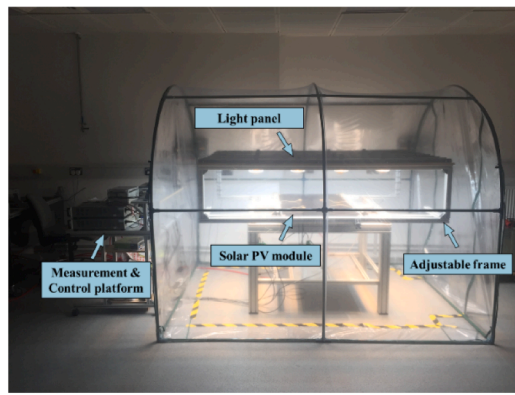
(a) Real diagram of the regulation system
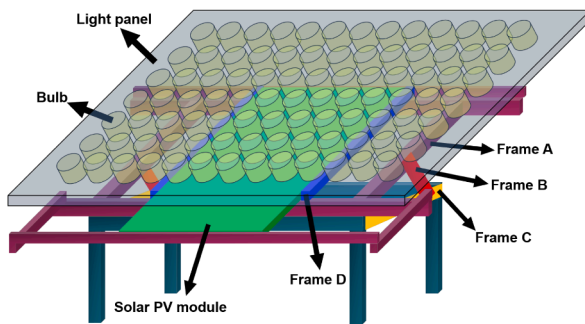
(b) Structure diagram of the regulation system

(c) Arrangement of the thermocouples

Fig. 6. Experimental facilities.

(a) and 6(b), a demonstration regulation system was developed and tested for monocrystalline PV panels operating in an arid climate. The light panel consisting of bulbs with different spectrums can simulate the radiation from the sunlight to the PV module. The tilting angle of the solar panel can be regulated by the adjustable frames A, B, and C, and the panel surface was always keeping the same parallel distance to the light panel. Frame D was used to fix solar panels and the total dimension of panel surface that can be tested was 1.3 m × 1.2 m. The main function of the measurement and control platform was to learn the variation of the power output and temperature of PV modules and regulate the airflow from the tank by controlling a solenoid valve. Referring to Fig. 6 (c), 8 thermocouples (**A-H**) were installed at the top and back side of the PV panel respectively to measure the average temperature of the module, which is

$$T_s = \left(\sum_{i=A}^{H} T_{Top}^i + \sum_{i=A}^{H} T_{Back}^i \right) \Bigg/ 16$$

The specific parameters related to the test rig were given in Table. 1.

Table 1
Parameters of the test rig.

Item	Value
Light maximum irradiation (W m^{-2})	490
Relative Humidity (%)	21
PV nominal power (W)	100
Panel dimension $L \times W \times H$ (m)	1.211 × 0.629 × 0.003
Surface roughness RMS (m)	0.4 × 10^{-6}
Density of the panel surface (kg m^{-3})	2.3 × 10^3
Specific heat of the panel surface (kJ kg^{-1})	0.75
Tilting angle (°)	0–60
Air tank volume (m^3)	0.34
Compressed air pressure (MPa)	0.1–1
Pressure range of solenoid valve (MPa)	0–1

4. Results and discussion

Design and control of a compressed air system for the PV arrays (composed of 12 panels described in the test rig) serving in an arid region of northwestern India was conducted. Referring to Fig. 7, the average size of the dust deposited on the panel surface was 20 μm and almost 90% of particles had diameters less than 30 μm (Nahar and Gupta, 1990; Bergin et al., 2017). The tilting angle of the panel was set to 30° and the average temperature of the surface can reach up to 333 K.

4.1. Validation

The components influenced the experiment results including the uncertainties in the measurement of PV voltage (U_1) and current (U_2), panel temperature (U_3), air flowrate (U_4), and time (U_5). As shown in Table 2, the standard uncertainties related to the components were obtained according to the verification report of the sensors and measuring devices.

(a) Cleaning

As shown in Table. 3, talcum mainly composed of SiO$_2$ with an average diameter of 20 μm was adopted and deposited evenly on the panel through a sieve. The deposition rate of the particle was set as 0.5 × 10^{-3} kg m^{-2} per day, and as shown in Fig. 8(a), the panel surface was covered by 5.3 g dust after two week-period operation. This led to a power drop of the tested PV module from 42.50 to 37.50 W at 303 K (PV load = 90 Ω). Referring to Fig. 8(b), two fan nozzles were installed on the top edge of the panel aiming to clean the whole panel surface using an airflow with an average thickness of 5 mm. To avoid the re-deposition of dust after the detachment, air blowing was implemented 5 s to remove the detached dust out of the panel surface under a flowrate of 1,370 L min^{-1} which was determined by the modelling work presented in Section 2.1. Then the power output of PV was measured again at 303 K after
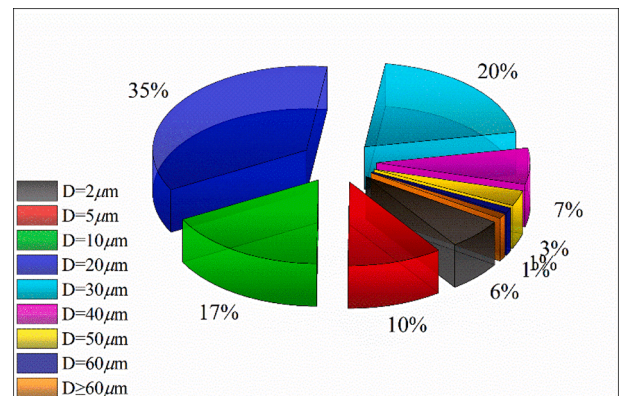

Fig. 7. Mass size distribution of the dust on the PV panel.

Table 2
Standard uncertainties for the components.

U_1 (%)	U_2 (%)	U_3 (°C)	U_4 (%)	U_5 (%)
0.1	0.1	0.5	1	0.1

4.2. Design and control

The parameters related to the dust on the panel surface in the arid region of northwestern India were: $E_{abs} = E_{scat} = 0.02$ m^2 g^{-1} and $\beta = 0.02$ (Bergin et al., 2017). According to Eq. (18), the reduction rate of
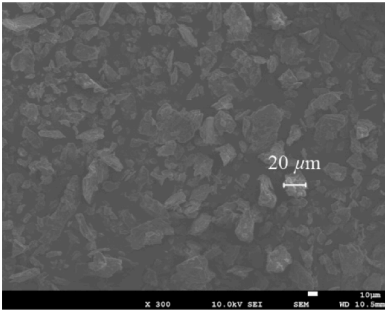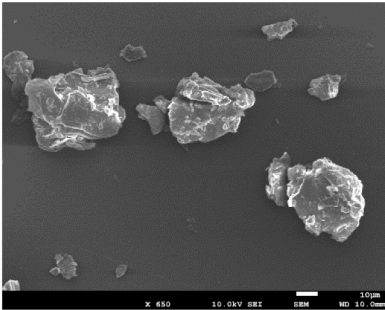
cleaning. To mitigate the effect of remaining dust on the evaluation of cleaning rate, the residual dust was cleaned completely by wiping after each test. The test was repeated three times and the results were shown in Table. 4.

After cleaning, the power output of the PV module recovered to an average of 41.82 W and, according to Eq. (20), the cleaning rate reached 86.4%. The reasons for not achieving full power recovery can be illustrated in four aspects. Firstly, although most areas of the panel surface can be cleaned by the airflow, dead ends depicted in Part A, Fig. 8(b) exist at current nozzle arrangement. Secondly, arising from the air expansion along the panel, the air thickness in Part B, Fig. 8(b) was larger than the average value determined by the design parameters of the nozzle. It resulted in the velocity in this part was not high enough to detach the particles from the panel surface. Thirdly, the actual particles smaller than 20 μm in the sample may not have been removed. Last but not least, underestimation of the VdW force may happen for some particles on the surface where a smaller roughness was superimposed on the larger-hemisphere roughness (Rabinovich et al., 2000a, 2000b). Dust particles that were not removed by these four causes blocked the irradiation and continued to reduce the power output of the PV module. It is worth noting that, many finer particles will be settled on the panel surface in aerosol deposition while larger particle size can be found in the sieving method owing to the agglomerate formulation (Guo et al., 2018). Therefore, a slight decrease of the cleaning rate may be predicted in the field application comparing with that in the laboratory test using sieve deposition.

(b) Cooling

Referring to Fig. 9(a), when the clean panel was heated up from 303 to 333 K, the power output of the module decreased from 42.50 to 28.24 W. Then an airflow at 1,370 L min^{-1} (297 K) was released to cool down the panel surface. From the cooling results shown in Fig. 9(b), after 130-second cooling, the average panel temperature dropped to 315 K and the power output increased to 32.42 W. R-square value of fitting the measured temperature and simulated one obtained by Eq. (24) was 0.978.

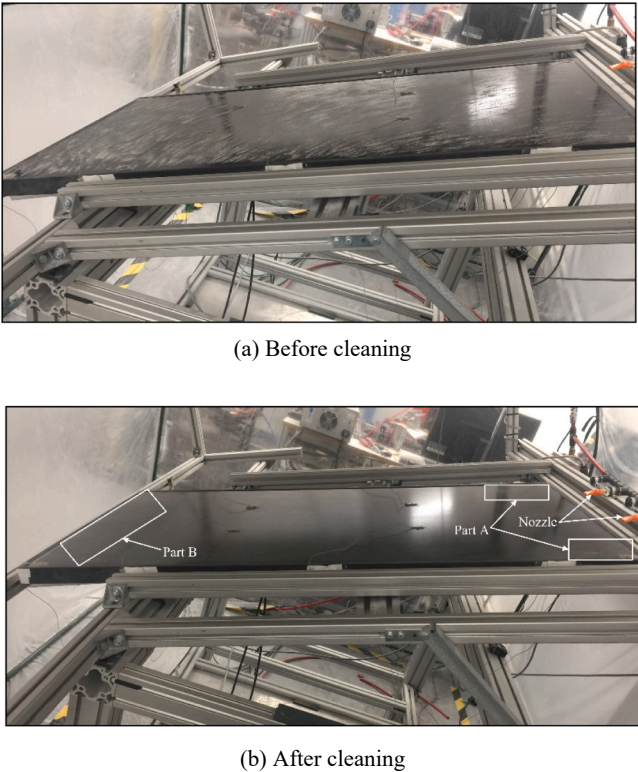(a) Before cleaning

(b) After cleaning

Fig. 8. PV panel surface before and after cleaning.

Table 4
Experiment results for cleaning.

Item	Soiled	Cleaned (Test 1)	Cleaned (Test 2)	Cleaned (Test 3)	Average
Flow rate (L min^{-1})	–	1402	1365	1368	1378
PV power (W)	37.50	41.91	41.73	41.80	41.82

Table 3
Properties of dust.

Item	Dust
SEM image	A. (×300) B. (×650)
Composition (Mineralogy Database)	SiO$_2$ (63.37%), MgO (31.88%), H$_2$O (4.75%)
Density (kg m^{-3})	2.7×10^3

(a) Heating

(b) Cooling

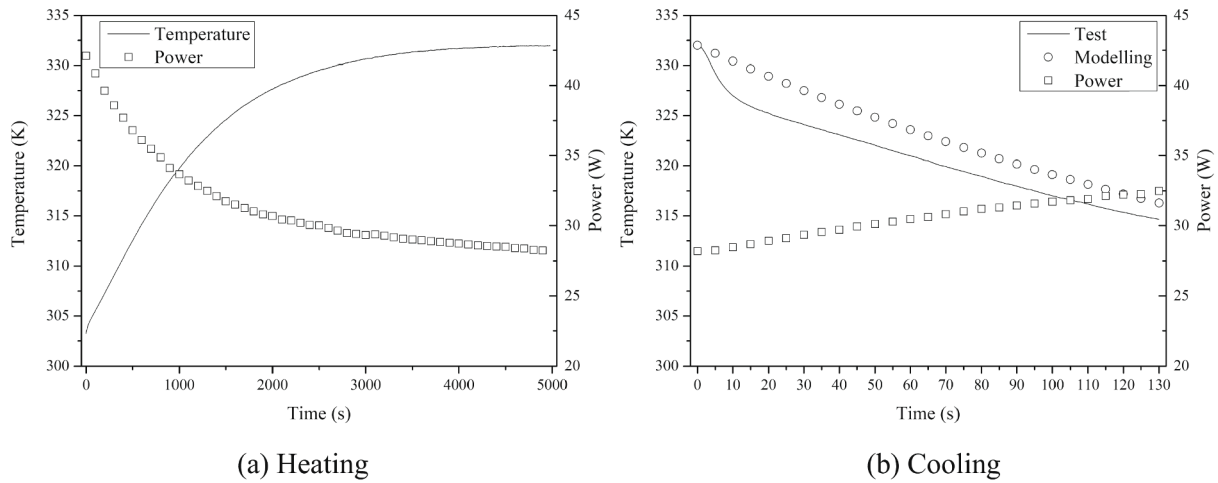**Fig. 9.** PV performance in the process of heating and cooling.

the transmittance of the solar energy caused by the dust deposition was $-4\%~g^{-1}~m^{-2}$. Taking the deposition rate of the dust as 0.5×10^{-3} kg m^{-2} per day, after two week-operation, the power output of the PV module dropped by 28% compared to that from the clean panel. On the other hand, when the temperature of the surface reached up to 333 K, the corresponding output power of the clean PV module dropped to 60 W ($\eta = 0.6\%~K^{-1}$) (Assi et al., 2012).

Using the same nozzle mechanism shown in Fig. 8 for each solar panel, to clean up dust particles from the size of 2 μm, the required initial pressure in the air tank under different blowing time and tank volume was obtained to inform the design of the compressed air system. Referring to Table 5, it can be learned that more initial air pressure was needed with the increase of blowing time and the reduction of tank volume. Taking the cleaning rate as 86.4% based on the experiment results, the performance improvement of a solar PV panel was studied and depicted in Fig. 10. After 10-second air blowing, the power output from the PV arrays increased from 567.4 to 741.5 W where the contribution of cleaning and cooling was 75.7% and 24.3% respectively. When the blowing time extended to 15 s and 20 s, the PV power improved to 758.2 W and 772.5 W, and the contribution of the cooling increased to 30.9% and 35.7%.

From the energy perspective, power consumption for producing the compressed air needs to be compared to the energy gain from the PV modules by the cleaning and cooling effects. Two following aspects influencing the energy Return of Investment (ROI) which can be calculated by the Eq. (30) were investigated to inform the formulation of an optimal control strategy.

$$\text{ROI} = \frac{W_{\text{gain}}}{W_{\text{cons}}} \tag{30}$$

where W_{gain} is the energy gain from cleaning and cooling effects. To facilitate the analysis, W_{gain} was referring to additional energy obtained before the reduction rate of the PV output by the dust deposition back to 28%.
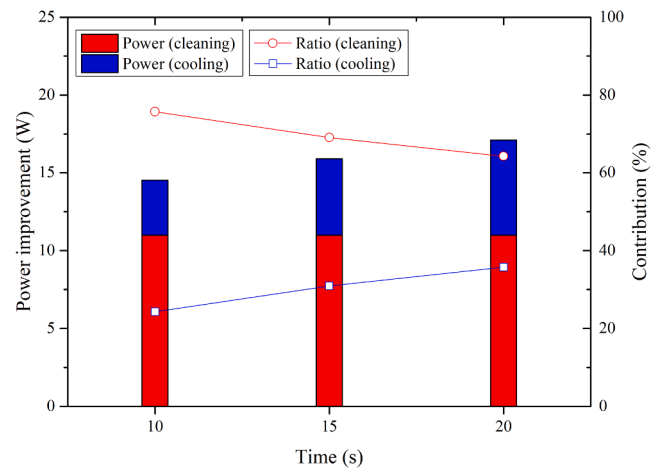

Fig. 10. Contribution of cleaning and cooling on performance improvement of a solar PV panel.

(a). Blowing duration

When the tank volume was set as 1 m³, and $\eta_{\text{comp}} = 0.8$ and $\eta_{\text{motor}} = 0.98$, the comparison of the energy consumption and gain from compressed-air regulation was conducted under different air blowing duration to clean up 2 μm-dust particles. A linear increase of dust deposition on the panel surface after cleaning was assumed and the reheating rate of the panel by the solar radiation (twice the radiation from the light panel in the test rig) after cooling was set as 0.5 K min⁻¹ according to the test results shown in Fig. 9(a). Referring to Fig. 11(a), the power improvement of the PV arrays increased from 0.17 kW to 0.19 and 0.21 kW when the blowing time extended from 10 s to 15 and 20 s because of the strengthening of cooling effect. The corresponding

Table 5
Parameters of the compressed air system.

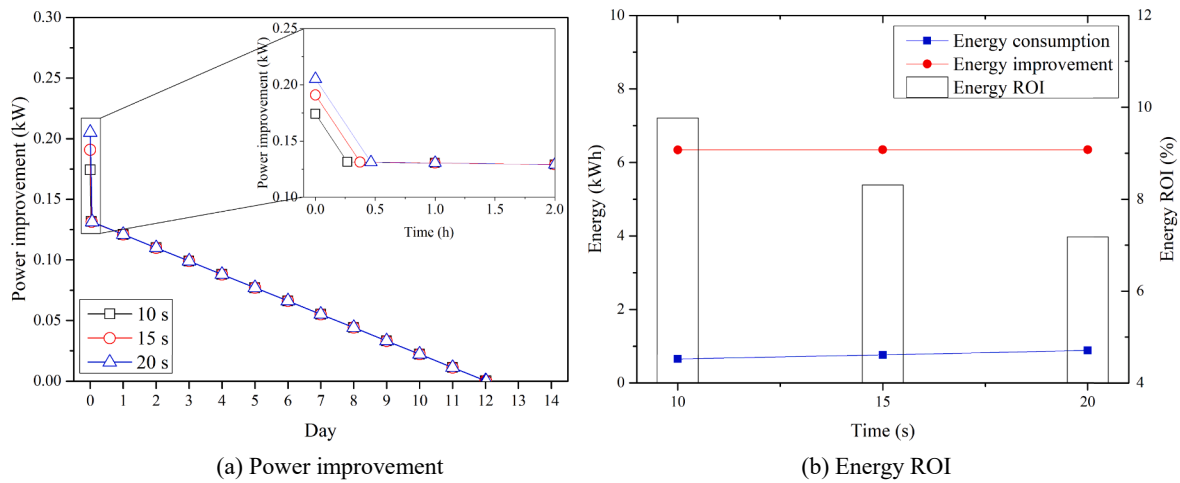| Item	$\Delta t = 10$ s			$\Delta t = 15$ s			$\Delta t = 20$ s		
Nozzle pressure (MPa)	0.3								
Airflow thickness (m)	5×10^{-3}								
Pipeline length (m)	2								
Pipeline diameter (m)	3×10^{-2}								
Tank temperature (K)	303								
Tank volume (m³)	1	1.5	2	1	1.5	2	1	1.5	2
Initial pressure P_0 (MPa) $\geq$	0.66	0.61	0.59	0.72	0.66	0.62	0.79	0.70	0.66

(a) Power improvement

(b) Energy ROI

Fig. 11. Energy analysis for different blowing time (sunlight time = 8 h per day).

temperature of the solar panel after cooling was 325.0, 321.8, and 319.1 K. However, as shown in 11(b), the energy ROI decreased from 9.8 to 8.3 and 7.2. The reason for this situation was the maintaining time of the cooling effect (i.e. tens of mins) had a much lower order of magnitude than that of the cleaning effect (i.e. more than 10 days) and the energy gain from the extension of the cooling process was much lower than the energy consumption for producing required airflow.

(b). Size of cleaning dust

Referring to Fig. 5, cleaning larger dust particles needs lower air velocity which leads to less air consumption. When the air blowing time and tank volume was set as 10 s and 1 m³, the energy consumption of the compressor and improvement of PV performance from removing different size of dust and accompanying cooling were compared. As shown in Fig. 12(a), the more dust on the panel surface was cleaned, the more PV power output can be achieved. However, it can be learned from Fig. 12(b), removing dust from the size of 10 μm would lead to a better energy ROI comparing with cleaning the smaller particles at the same time. With further increase of the initial cleaning size, the ROI decreased gradually, and no energy profit was available when the cleaning started from dust larger than 40 μm.
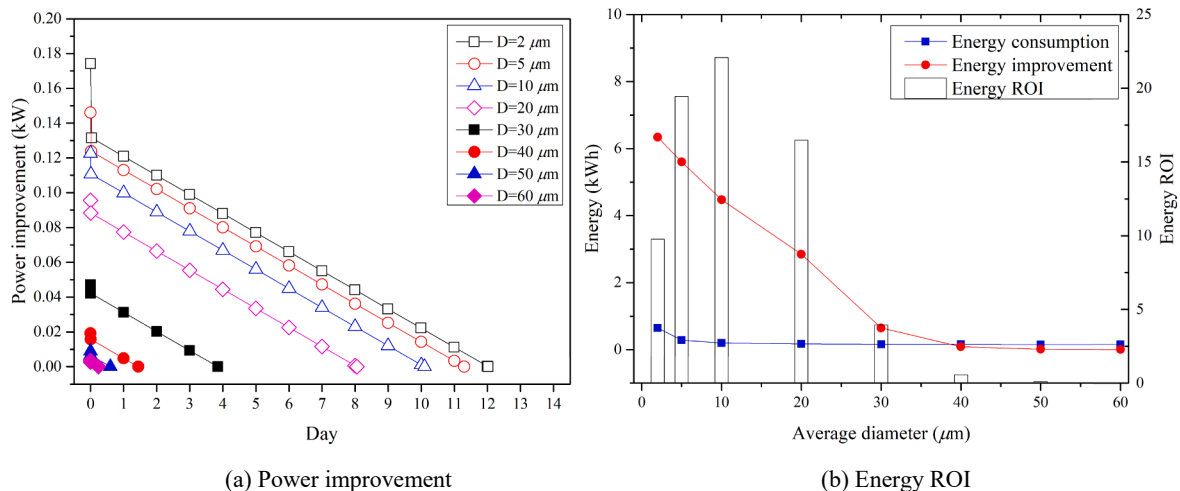
5. Conclusion

Cleaning and cooling of a solar Photovoltaic (PV) panel using compressed airflow was studied and tested in this paper for the improvement of PV performance. Modelling work of the dust adhesion and detachment was conducted first to obtain the airflow rate to clean the dust particles. Then the temperature variation of the panel surface during the cleaning process was analysed to evaluate the accompanying power increase by the cooling effect. Dynamic modelling of the tank pressure in the discharging process was established to decide the tank volume and operation time of the compressed air system.

To demonstrate the effectiveness of the proposed modelling and system, an experimental rig was established for the monocrystalline PV modules operating in the arid climate. The power improvement of the PV panel through cleaning and cooling was validated. The cleaning rate from the current nozzle structure could reach 86.4% and R-square value for the temperature modelling fitting was 0.978. Based on the test results, the design and control of a regulation system for the PV arrays (12 panels) operating in an arid region of northwestern India were investigated. When the blowing time was set as 10, 15, 20 s, the power output of the PV arrays increased from 567.4 W by 30.7, 33.6, and 36.1% respectively. To develop an optimal control strategy for maximising energy profit, the influence of the air blowing duration and dust cleaning size on the energy Return of Investment (ROI) was investigated. On the one hand, although the release of airflow could continuously cool down

(a) Power improvement

(b) Energy ROI

Fig. 12. Energy analysis for different cleaning size of dust (sunlight time = 8 h per day).

the panel surface and increase the PV power after cleaning, the ROI would decrease because the cooling effect can only maintain a relatively short time comparing to the cleaning effect and therefore the energy used for producing required airflow was much higher than the energy benefit from an increased cooling duration. On the other hand, cleaning particles including those with small size and mass would contribute to higher PV power output, however, may decrease system ROI because of the increase of energy consumption for the required detachment flow-rate. Therefore, the blowing time and specific particle size for removals need to be determined considering the optimal balance between energy consumption in compressing air and energy gain from PV performance improvement for the application scenario studied.

This study could provide theoretical guidance and an experimental basis to design a regulation system using compressed air for boosting the performance of solar PV installations and develop an optimal control strategy to maximise energy profit. The results would help improve the efficiency of renewable energy utilisation and reduce the emission of greenhouse gas from the energy industry.

6. Prospective

Based on the current research progress, future work for further improvement of solar PV performance using compressed air-based regulation system are as follows:

- The mechanism of the nozzle (number, position, angle, etc) needs to be updated to increase the cleaning rate of airflow.
- Maximum Power Point Tracking (MPPT) under different dust deposition rate and temperature of the PV panel needs to be integrated to further improve the PV efficiency.
- For the long-term operation of PV arrays, the frequency and time of the regulation should be optimised considering the variation of solar radiation and load demand, and weather conditions, etc, to achieve more energy benefit and economic gain.

Declaration of Competing Interest

The authors declare that they have no known competing financial interests or personal relationships that could have appeared to influence the work reported in this paper.

Acknowledgements

References

Adinoyi, M., Said, S., 2013. Effect of dust accumulation on the power outputs of solar photovoltaic modules. Renew. Energy. 60, 633–636.

Ahmadi, G., Guo, S., 2007. Bumpy particle adhesion and removal in turbulent flows including electrostatic and capillary forces. J. Adhes. 83, 289–311.

Ahmadi, G., Guo, S., Zhang, X., 2007. Particle adhesion and detachment in turbulent flows including capillary forces. Part Sci Technol. 25, 59–76.

Alagoz, S., Apak, Y., 2020. Removal of spoiling materials from solar panel surfaces by applying surface acoustic waves. J. Cleaner Prod. 253, 119992–120067.

Al-Housani, M., Bicer, Y., Muammer Koç, M., 2019. Experimental investigations on PV cleaning of large-scale solar power plants in desert climates: Comparison of cleaning techniques for drone retrofitting. Energy Convers. Manage. 185, 800–815.

Assi, A., Hassan, A., Al-Shamisi, M., Hejase, H., 2012. Removal of air blown dust from Photovoltaic arrays using forced air flow of return air from air conditioning systems.

In: International conference on renewable energies for developing countries. REDEC 2012.

Bergin, M., Ghoroi, C., Dixit, D., S., Schauer, J., Shindell, D., 2017. Large reductions in solar energy production due to dust and particulate air pollution. Environ. Sci. Technol. Lett. 4, 339–344.

Brambilla, S., Speckart, S., Brown, M., 2017. Adhesion and aerodynamic forces for the resuspension of nonspherical particles in outdoor environments. J. Aerosol Sci. 112, 52–67.

Burdick, G., Berman, N., Beaudoin, S., 2005. Hydrodynamic particle removal from surfaces. Thin Solid Films. 488, 116–123.

Carello, M., Mazza, L., Alexandre Ivanov, A., 1998. Pressure drop in pipe lines for compressed air: comparison between experimental and theoretical analysis. Trans. Eng. Sci. 18, 35–44.

Chesnutt, J., Ashkanani, H., Guo, B., Wu, C., 2017. Simulation of microscale particle interactions for optimization of an electrodynamic dust shield to clean desert dust from solar panels. Sol. Energy 155, 1197–1207.

Crowley, J., 2008. Simple expressions for force and capacitance for a conductive sphere near a conductive Wall. In: Proc. ESA Annual Meeting on Electrostatics, Paper D1.

Du, X., Jiang, F., Liu, E., Wu, C., Ghorbel, F., 2019. Turbulent airflow dust particle removal from solar panel surface: Analysis and experiment. J. Aerosol Sci. 130, 32–44.

Figgis, B., Nouviaire, A., Wubulikasimu, Y., Javed, W., Guo, B., Ait-Mokhtar, A., Belarbi, R., Ahzi, S., Yves Rémondb, Y., Ahmed Ennaoui, A., 2018. Investigation of factors affecting condensation on soiled PV modules. Sol. Energy 159, 488–500.

Goldman, A., Cox, R., Brenner, H., 1967. Slow viscous motion of a sphere parallel to a plane wall-II Couette flow. Chem. Engng Sci. 22, 653–660.

Guo, B., Javed, W., Pett, C., Wu, C., Scheffe, J., 2018. Electrodynamic dust shield performance under simulated operating conditions for solar energy applications. Sol. Energy Mater Sol. Cells 185, 80–85.

Gupta, V., Sharma, M., Pachauri, R., Badu, K., 2019. Comprehensive review on effect of dust on solar photovoltaic system and mitigation techniques. Sol. Energy 191, 596–622.

Hamaker, H., 1937. The London-Van der waals attraction between spherical particles. Physica 4, 1058–1072.

Hartmann, N., Vöhringer, O., Kruck, C., EltropIlse, L., 2012. Simulation and analysis of different adiabatic Compressed Air Energy Storage plant configurations. Appl. Energy. 93, 541–548.

Hinds, W., 2012. Aerosol technology: properties, behavior, and measurement of airborne particles. Wiley.

Ilse, K., Werner, M., Naumann, V., Figgis, B., Hagendorf, C., Bagdahn, J., 2016. Microstructural analysis of the cementation process during soiling on glass surfaces in arid semi-said climates. Phys. Status Solid RRL 10, 525–529.

Ilse, K., Figgis, B., Naumann, V., Hagendorf, C., Bagdahn, J., 2018. Fundamentals of soiling processes on photovoltaic modules. Renew. Sustain. Energy Rev. 98, 239–254.

Incropera, F., DeWitt, D., Bergman, T., Lavine, A., 2006. Fundamentals of heat and mass transfer. John Wiley and Sons, New York.

Jiang, Y., Lu, L., Ferro, Andrea R., Ahmadi, G., 2018. Analyzing wind cleaning process on the accumulated dust on solar photovoltaic (PV) modules on flat surfaces. Sol. Energy 159, 1031–1036.

Kawamoto, H., Guo, B., 2018. Improvement of an electrostatic cleaning system for removal of dust from solar panels. J. Electrost. 91, 28–33.

Kawamoto, H., 2020. Improved detachable electrodynamic cleaning system for dust removal from soiled photovoltaic panels. J. Electrost. 107, 103481.

Li, Q., Rudolph, V., Peukert, W., 2006. London-van der Waals adhesiveness of rough particles. Powder Technol. 161, 248–255.

Malik, A., Damit, S., 2003. Outdoor testing of single crystal silicon solar cells. Renew Energy. 28, 1433–1445.

Mazumder, M., Sharma, R., Biris, A., Zhang, J., Calle, C., Zahn, M., 2007. Self-cleaning transparent dust shields for protecting solar panels and other devices. Part. Sci. Technol. 25 (1), 5–20.

Middle east solar industry association, 2020. Solar outlook report 2020.

Mineralogy Database, Talc mineral data. http://webmineral.com/data/Talc.shtml#.YD9wqmj7SUn [Accessed 2 March 2021].

Moharram, K., Abd-Elhady, M., Kandil, H., El-Sherif, H., 2013. Influence of cleaning using water and surfactants on the performance of photovoltaic panels. Energy Convers. Manage. 68, 266–272.

Moutinho, H., Jiang, C., To, B., Perkins, C., Muller, M., Al-Jassim, M., Simpson, L., 2017. Adhesion mechanisms on solar glass: Effects of relative humidity, surface roughness, and particle shape and size. Sol. Energy Mater Sol. Cells 172, 145–153.

Nahar, N., Gupta, J., 1990. Effect of dust on transmittance of glazing materials for solar collectors under arid zone conditions for India. Solar and Wind Technology 7, 237–243.

Rabinovich, Y., Adler, J., Ata, A., Singh, R., Moudgil, B., 2000a. Adhesion between nanoscale rough surfaces I. Role of asperity geometry. J. Colloid Interface Sci. 232, 10–16.

Rabinovich, Y., Adler, J., Ata, A., Singh, R., Moudgil, B., 2000b. Adhesion between nanoscale rough surfaces II. Measurement and Comparison with Theory. J. Colloid Interface Sci. 232, 17–24.

Rumpf, H., 1990. Particle technology. Chapman & Hall, London/New York.

Said, S., Hassan, G., Walwil, H., Al-Aqeeli, N., 2018. The effect of environmental factors and dust accumulation on photovoltaic modules and dust-accumulation mitigation strategies. Renew. Sustain. Energy Rev. 82, 743–760.

Sayigh, A., Al-Jandal, H., Ahmed, H., 1985. Dust effect on solar flat surfaces devices in Kuwait. In: Proceedings of the Workshop on the Physics of Non-Conventional Energy Sources and Materials Science for Energy, pp. 353–367.

Shariah, A., Al-Akhras, M., Al-Omari, I., 2002. Optimizing the tilt angle of solar collectors. Renew. Energy 60, 587–598.

Williams, R., Tanimoto, R., Simonyan, A., Fuerstenau, S., 2007. Vibration characterization of self-cleaning solar panels with piezoceramic actuation. In: Proceedings of the Collect. Tech. Pap. Struct. Dyn. Mater. Conf., vol. 1, pp. 512–520.